2

Single-Molecule Analysis of Biomembranes

Thomas Schmidt and Gerhard J. Schütz

Abstract Biomembranes are more than just a cell's envelope – as the interface to the surrounding of a cell they carry key signalling functions. Consequentially, membranes are highly complex organelles: they host about thousand different types of lipids and about half of the proteome, whose interaction has to be orchestrated appropriately for the various signalling purposes. In particular, knowledge on the nanoscopic organization of the plasma membrane appears critical for understanding the regulation of interactions between membrane proteins. The high localization precision of ∼20 nm combined with a high time resolution of ∼1 ms made single molecule tracking an excellent technology to obtain insights into membrane nanostructures, even in a live cell context. In this chapter, we will highlight concepts to achieve superresolution by single molecule imaging, summarize tools for data analysis, and review applications on artificial and live cell membranes.

2.1. Introduction

From the beginning of cell biology, biomembranes have been considered to be of major relevance for cellular function. Each cell is separated from its environment via a biomembrane. Membranes enable the division of the cell cytoplasm into chemically distinct subspaces, thereby governing the development of cell organelles. Moreover, they act as a matrix for integral, lipid-anchored, or peripheral membrane proteins and thereby considerably affect protein function.

The role of lipids as the major constituents of biomembranes was established in the 1970s, leading to the proposal of the fluid mosaic model for the plasma membrane [1]. According to this model, it is the lipids and not the proteins that constitute the matrix of the cell membrane. Since this matrix was shown to be in a fluid state, integral membrane proteins were expected to be free to diffuse laterally within the membrane, as long as no interaction with cytoskeletal elements hinders their Brownian motion. The relevance of lipid bilayers for cell biology initiated a vast number of studies on artificial systems, which aimed at the structural characterization of bilayers and monolayers under various environmental conditions [2].

T. Schmidt • Physics of Life Processes, Leiden Institute of Physics, Leiden University, Niels Bohrweg 2, 2333 CA Leiden, The Netherlands
G. J. Schütz • Biophysics Institute, Johannes Kepler University Linz, Altenbergerstr. 69, A-4040 Linz, Austria

P. Hinterdorfer, A. van Oijen (eds.), *Handbook of Single-Molecule Biophysics*,
DOI 10.1007/978-0-387-76497-9_2,

The restriction to the study of artificial systems allowed for full control over parameters such as lipid composition, lateral pressure, temperature, and ionic strength.

In particular, there has been increasing interest in obtaining detailed understanding of the structure and dynamics of the cellular plasma membrane itself [3], primarily based on recognition of its essential role in controlling cellular signaling processes. In recent years a picture has emerged that ascribes to the plasma membrane a high degree of organization at very short length scales of tens of nanometers [4–7]. Experiments performed on single biomolecules have added to this picture by providing access to spatial information below the diffraction limit of classic light microscopy.

A biomolecule moving in an artificial or cellular lipid membrane may experience multiple forces that influence its characteristic motion. In consequence, the path will deviate to a greater or lesser extent from a Brownian trajectory. Deviations from free diffusion may be caused by (1) the confinement of the tracer molecule in a meshwork of permeable barriers, resulting in hop diffusion [8]; (2) the transient binding of the tracer to an (immobile) membrane structure, yielding short periods of altered—generally reduced —mobility [9,10]; (3) periods of active transport via motor proteins [11]; (4) direct or indirect anchorage to the cytoskeleton, yielding immobilization or tethered motion of the tracer [12]; (5) fixed obstacles at high surface density [13]; and (6) the partitioning of the tracer to mobile or immobile membrane domains ("rafts") [14,15].

In the following we distinguish two strategies for following a single biomembrane constituent. Historically the first approach was termed *single-particle tracking (SPT)*, in that the molecule of interest was linked specifically to a larger particle that gave sufficient signal to be detectable as an individual point light source over multiple frames [16–25]. Single particles can be imaged with high signal-to-noise ratio, and therefore the location can be determined with high precision far beyond the limit of diffraction [23,26]. There is hardly any limit to the length of such a trajectory because no photophysical damage occurs to the traced particles. Termination may yet occur when using quantum dots for labeling. Due to inherent blinking [27], there will be dark periods in a trajectory; if the dark interval gets too long, correlation with the next appearance may be difficult.

The second approach was based on the attempt to further reduce the size of the label down to the ultimate limit of an *individual dye molecule*. These endeavors were based on the concern that larger particles might interfere with the motion and function of the tracer molecule. Pioneering studies in the mid 1990s demonstrated that single dye molecules indeed provide sufficient signal for imaging with subpixel localization precision and tracking over multiple frames [28–31]. Further technological advances, as well as improved understanding of the biological systems, have led to an increase in studies both on artificial membranes [32–39] and the live cell plasma membrane [40–61]. In contrast to particles, however, dye molecules are affected by prolonged excitation, which results in the photobleaching of the probe and the concomitant termination of the trajectory [62].

We focus in this chapter on reviewing analytical tools for the analysis of single-molecule tracking experiments in biomembranes and describe applications to artificial membranes and the live cell plasma membrane; the emphasis is on single-dye approaches. Initially, we discuss concepts of superresolution imaging based on single-molecule detection.

2.2. Superresolution

The major advantage of single-molecule approaches for biomembrane research is the enormous potential for characterization of subwavelength membrane structures. To

elucidate superresolution concepts for membrane research, we first briefly sketch the imaging constraints. An isotropic emitter (fluorescent bead or quantum dot) or scatterer (gold particle) will be imaged according to the point spread function of the imaging device, which is well approximated by an Airy disk of radius $\rho = 0.61 \times \lambda/NA$, with λ the imaging wavelength and NA the numerical aperture [63]. A single dye molecule with fixed emission dipole orientation will emit photons depending on its three-dimensional (3D) orientation in space, which in general leads to a significantly altered image [64]. In the case of a rapidly rotating molecule the contributions of the individual orientations add up, thereby yielding an image given by the point spread function. Since in fluid biomembranes the constituents show rapid rotation on a nanoseconds time scale [35], an approximation of the image by the point spread function centered on the actual position is justified.

The nonzero width of the Airy disk represents the basic limitation to the resolving power of the apparatus used. Imaging of an arbitrary object can be described by

$$f'(\vec{r}) = \int_{-\infty}^{-\infty} f(\vec{s})\,\delta(\vec{r}-\vec{s})\,d\vec{s} \Rightarrow \int_{-\infty}^{-\infty} f(\vec{s})\,psf(\vec{r}-\vec{s})\,d\vec{s} = g(\vec{r})$$

with $f'(\vec{r})$ representing the fluorescent object, which is described as a sum of point light sources, each of which is imaged according to the point spread function (PSF), yielding the total image $g(\vec{r})$; the arrow denotes the imaging processes. If we assume a Gaussian approximation for the PSF, a sample labeled with dyes at positions $\vec{s}_i$ would yield the image

$$g(\vec{r}) = \sum_i N_i \frac{1}{2\pi\rho^2} \exp\left(-\frac{(\vec{r}-\vec{s}_i)^2}{2\rho^2}\right)$$

where N_i is the number of photons emitted per dye. As a consequence, two point light sources with a distance smaller than ρ would yield highly overlapping images and thus could not be resolved as individual objects. This theorem, known as the "Abbe limit" or "Rayleigh criterion," is generally used to define resolution in light microscopy. Several modifications to standard imaging methods have been employed to obtain higher resolution via narrowing the point spread function by utilizing near-field effects [65,66], nonlinear excitation [67], by confocal excitation and detection schemes [68,69]. Recently, new concepts were introduced that use saturation effects when illuminating the sample with structured illumination [68,70,71] (see Ref. 72 for review).

Single–molecule imaging has enabled additional strategies for achieving superresolution. The general idea is to thin out the active probe such that signals become well separated and can be detected by classical diffraction-limited optics [73]. Then, a molecule can be localized to high precision of a few nanometers by determining the centroid of its image [26,64,74–76]. Different variants have been introduced to use this high localization precision for determination of molecular distances and for enhancement of imaging resolution in general (see Figure 2.1 for a sketch):

1. *Two-color imaging*. In the first approaches, different color channels were used to measure the distance between unresolvably close molecules of different spectrum [33,77,78]. Two-color imaging offers a way to sensitively detect colocalization between a ligand and its receptor in binding assays [79,80] and also in the live cell plasma membrane [10].
2. *Dynamic imaging*. Alternatively, one may exploit the time domain for diluting the biomolecule, for example, by allowing fluorescent ligands to bind and dissociate

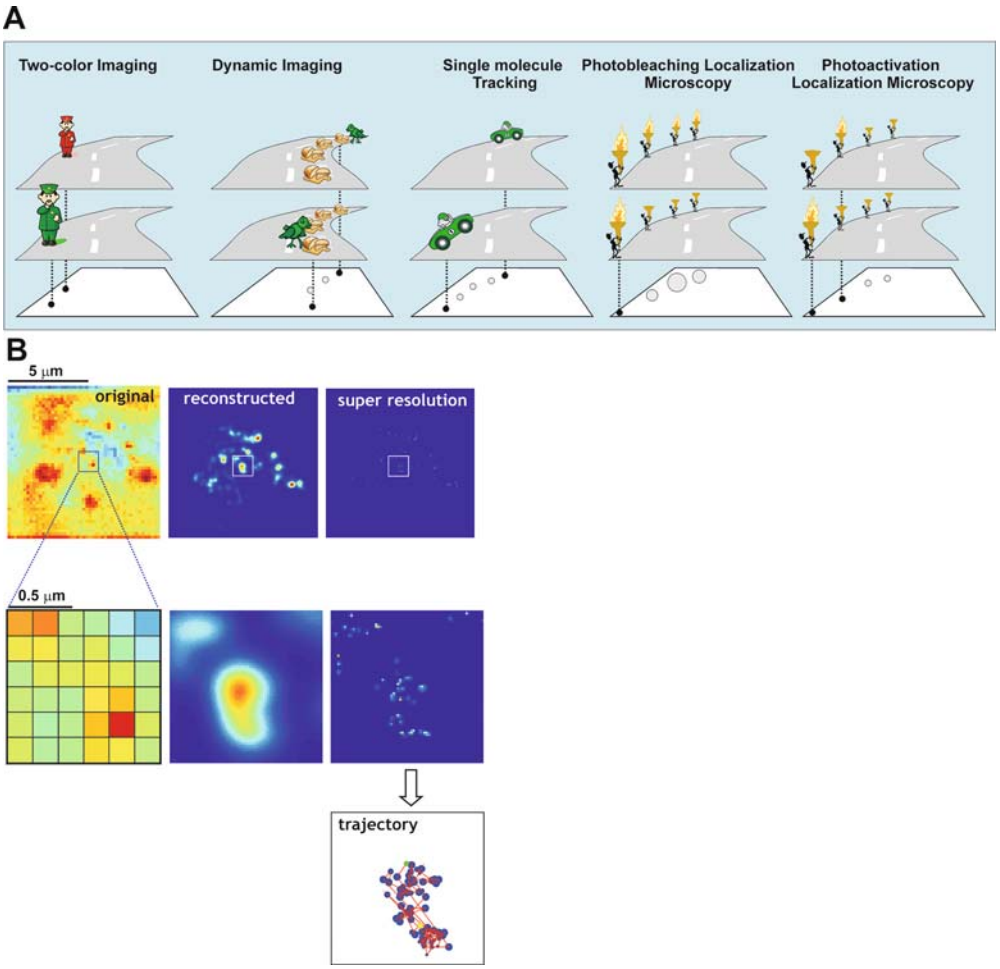

Figure 2.1. A. Concepts for achieving superresolution based on single-molecule imaging. The structure to be studied is represented as a road carrying different objects. The two top rows show two arbitrary observations of the system. The bottom row shows the results: The circles denote the detected single-molecule positions, and the size of the circles indicates the localization precision. See text for details on the individual approaches. **B.** The mean background-subtracted image taken from a stack of 500 images in an experiment described in Figure 2.2 exemplifies the construction of a superresolution image. Whereas the original mean image shows hardly any structure, the reconstructed image, as noise-free, indicates the existence of still-unresolved finer structure within the stack. The superresolution image resolves this structure given by the path of a moving molecule. The structure is better seen at 10× magnification (*lower image row*). In the right column, the single-molecule position data are plotted as Gaussians of widths given by the respective confidence limit of the positional fit. Such superresolution data can be subsequently used to construct molecular trajectories.

randomly from their receptors in the plasma membrane. If the applied concentration is low enough, single binding events can be detected and localized. An overlay of all determined positions provides a high-resolution map of the receptor organization in the plasma membrane [81].

3. *Single-molecule/particle tracking*. A similar strategy is based on the study of mobile molecules, which sample the accessible space within the biomembrane over time. Whenever structural features affect any measurable parameter of the molecule (e.g., its intensity, spectrum, the diffusion constant, or velocity), each trajectory can be

subdivided into distinct segments with a resolution only limited by the localization precision. This strategy has been used to identify, for example, step sizes of motor proteins [75,82] and confinements in artificial membranes [32] or in the cellular plasma membrane [40,46,56,57].

4. *Photobleaching localization microscopy.* To facilitate accurate determination of the positions of neighboring molecules with nanometer distance, Gordon and coworkers used photobleaching [83]: whenever a molecule within an assembly of subdiffraction dimension photobleaches, a concomitant shift in the signal distribution can be detected and used iteratively for the estimation of all dye positions. A similar approach has been used to determine the label positions on stretched DNA [84].
5. *Photoactivation or photoswitching localization microscopy*. Photobleaching localization microscopy is restricted to the analysis of weakly stained specimens because the localization analysis becomes inaccurate for a large number of dyes within a diffraction-limited spot. As an alternative, researchers have developed the inverse approach, which is based on the consecutive photoactivation, imaging, and photobleaching of a sample labeled with photoactivatable fluorophores (e.g., photoactivatable green fluorescent protein (paGFP) [85]) [86–88]. In this methodology, localization precision determines the resolution [89].

The listed approaches may all be applied for high-resolution biomembrane imaging; see the following sections for a detailed discussion of the individual examples. It should be noted, however, that all superresolution concepts—including the ensemble techniques described earlier —are comparably slow, in that they require addressing the pixels individually. More precisely, if two pixels are to be addressed simultaneously, they have to be separated at least by the width of the diffraction-limited point spread function. For two-dimensional (2D) microscopy, the minimum time required for recording an image at superresolution $T_{\min}$ is given by $T_{\min} = (\rho/\sigma_{xy})^2 t_{\text{frame}}$, with ρ the width of the point spread function, σ_{xy} the localization precision, and t_{frame} the time required for obtaining one frame; for example, recording an image at 10-times-improved resolution would require 100-fold longer recording times! If we further consider the imaging of dynamic structures moving with a diffusion coefficient D, the recording time should be faster than $T_{\max} \approx \text{resolution}^2/4D$, the time the molecule needs to move over one pixel. Superresolution imaging of dynamical processes would therefore actually require improved time resolution.

In contrast, tracking approaches do not necessarily lead to images; one can also use the information content of single trajectories to analyze structures that interfere with the motion of the tracer. In this case, the timing requirements are less strict: It may not even be necessary to image faster than the time the molecule needs to traverse the structure of interest. This advantage made single-particle/molecule tracking a preferred methodology in biomembrane research.

2.3. Detection and Tracking

The possibility of detecting individual fluorophores emerged in 1989 [90] with the detection of individual pentacene molecules at liquid-He temperatures in a confocal setting. Since then, the developments in optical dielectric filters and charge-coupled device (CCD) cameras has led to sensitivities that makes it possible to detect individual fluorophores in wide-field microscopy and at video rates in the living cell. The selective throughput of optical filters now approaches 90% at the same time blocking unwanted wavelengths by $>10^5$, and

the detection efficiency of back-illuminated CCD cameras is up to 95% throughout the whole visible spectral range. The reliable detection of molecules is hence just limited by the noise in acquisition governed by detector noise (which can be as low as 3 electrons per pixel root mean square (RMS) on a N_2-cooled CCD) and the sample background. Optimization in preparation protocols reduces the latter to basically zero for artificial systems (e.g., polymer films, biomimetic systems) and for cells observed in total internal reflection (TIR) mode, whereas for cells observed in regular wide-field applications the background is still substantial. Typically 30 counts per pixel per millisecond illumination at excitation intensity $\sim$1 kW/cm^2 is seen for live-cell wide-field applications. At those conditions about 100 counts are detected from an individual fluorophore [91]. A typical image is shown in Figure 2.2 ("original").

The sheer amount of data generated by such images requires a stable and unattended automatic analysis. In a first step any static or slowly varying background has to be subtracted. Techniques like high-order [4–8] polynomial fitting, low-spatial-frequency filtering, mean image calculation, and pixel-by-pixel low-temporal frequency filtering have been used to generate a reliable background image (Figure 2.2, "background"). The background-subtracted images are subsequently optimally filtered by cross-correlation with the PSF of the microscope approximated by a Gaussian (Figure 2.2, "target"). Thresholding of those optimally filtered images in which the threshold is dynamically adjusted to the image noise makes it possible reliably to identify signals that are above noise by a factor of >3 (Figure 2.2, "thresholded"). The final analysis then proceeds by fitting each of the identified signals to the PSF and extracting the information on position, signal strength, spatial width of the signal, and signal of the background, as well as an estimate on the accuracy in each of the parameters (Figure 2.2, "fitting"). Depending on the type of data, also 3D information can be retrieved. Within the Rayleigh length [$z_0 = \pi\lambda/(4\mathrm{NA}^2)$] the PSF widens with z position as $\omega(z) = \omega_0\sqrt{1 + z^2/z_0^2}$, which permits extraction of the z position [41]. For small deviations from the plane of focus (small z) it is advantageous to introduce a small astigmatism into the detection light path to increase the accuracy in determination of the z position [92]. The positional accuracy is further increased by taking fast image stacks, which are subsequently analyzed simultaneously. In this way the 3D position of an individual object is determined to within 30 nm in xyz, respectively, and image volumes of $10\times10\times10$ μm^3 are analyzed at frame rates of 10 sec^{-1} (Laurent Holtzer, unpublished results; [93]).

Image analysis as just described is the basis for further data treatment. It becomes possible to restrict further analysis to signals of, for example, a certain signal strength or a desired positional accuracy (Figure 2.2, "reconstructed"). In particular the latter is key for the novel nanometer-resolution microscopy methods described in the previous subsection. Correlations between the parameters can be used to obtain information on, for example, the aggregation state of the molecule or local differences in pH seen as a local change in signal strength.

In addition, temporal information from image movies together with the positional information is used to obtain trajectories of individual molecules. The generation of trajectories is straightforward for sparsely occurring and immobile objects [25,94]. However, in general we face the problem of correlating M mobile molecules in image n with L mobile molecules in image $n + 1$ (Figure 2.3). This is a classical NP-complete problem ("traveling salesmen") for which we follow an optimization procedure from operations research developed by Vogel. First a complete translational matrix is built up that includes the probability that molecule j in image i at position $r_{j,i}$ moves to molecule k in image $I + 1$ at position $r_{k,i+1}$ by diffusion as characterized by a diffusion constant D,

$$p(j,k) = \exp\left(-\frac{(\vec{r}_{j,i} - \vec{r}_{k,i+1})^2}{4Dt}\right)$$

In addition, molecules are allowed to disappear by diffusion out of the observed area or by photobleaching, $p(j,k > L) = p_{\text{bleach}}$, and molecules are allowed to move into the observed area or get reactivated, $p(j > M,k) = p_{\text{activation}}$. Subsequently trajectories are constructed that optimize for the total probability of all connections between two images,

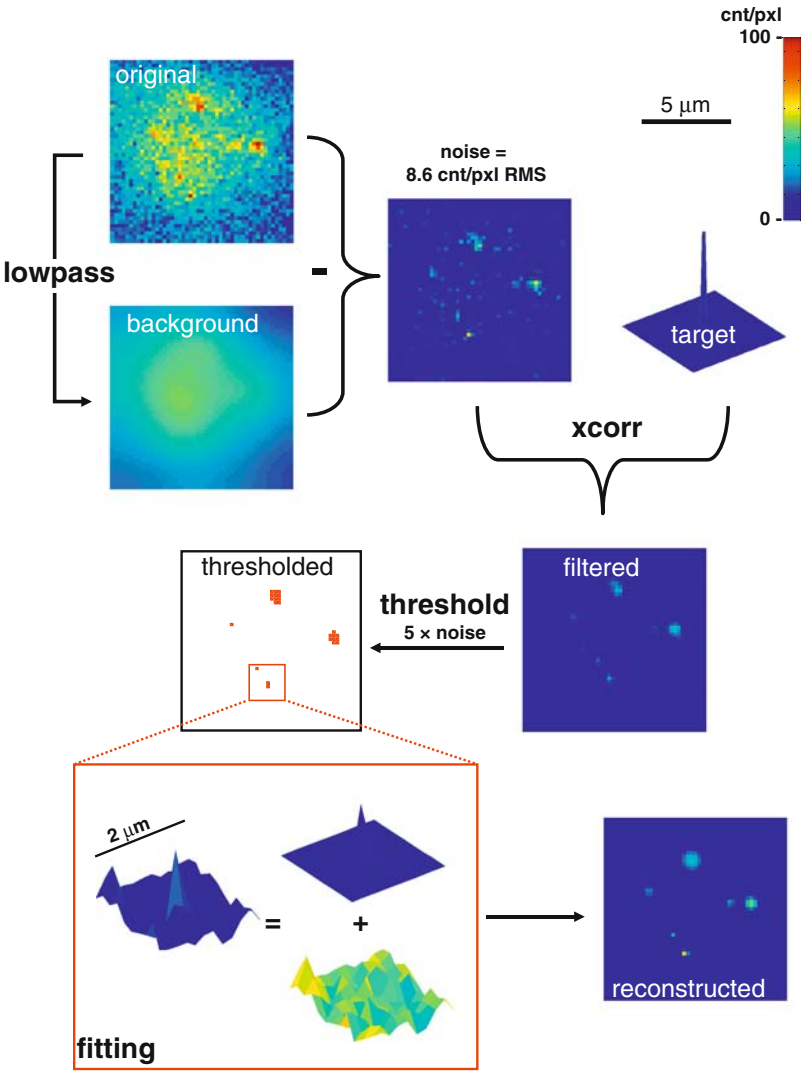

Figure 2.2. Steps in image analysis for automated single-molecule detection. *Dictyostelium* cells were transfected with a yellow fluorescent protein (YFP)–labeled cyclic adenosine monophosphate (cAMP) receptor located in the plasma membrane of the cells. The cells were illuminated at an intensity of 2 kW/cm^2 for 5 ms to create the images on a N_2-cooled charge-coupled device (CCD) camera. The images have a size of 10×10 µm^2. Low-pass filtering of the original image was used to create a smooth background image. The background-subtracted original image (noise: 8.6 counts/pixel root mean square) was subsequently cross-correlated (xcorr) by the Gaussian target image, leading to an optimally filtered image. Signals that exceed a threshold criterion are subsequently fitted to the Gaussian target image. Results of the fitting were used to obtain a noise-free reconstruction image.

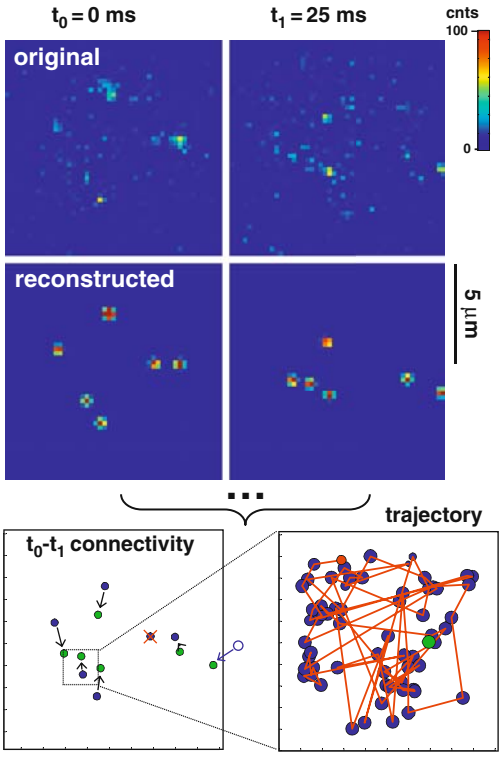

Figure 2.3. Two subsequent images (25-ms delay) from the experiment described in Figure 2.2 exemplify the construction of trajectories. A Vogel algorithm was used to obtain the connectivity map in which the various processes are visualized: (1) diffusion (*black arrows*), (2) bleaching (*red cross*), and (3) diffusion into the observation volume (*blue arrow*). The position of the molecules at t_0 are shown in blue, those at t_1 are shown in green. On the bottom right the trajectory of a single receptor is shown.

$\log(P) = \sum_{j,k} \log(p(j,k))$. This algorithm enhances the number of faithfully reconstructed trajectories even in the case of a sizable amount of molecules per image.

Since one step in trajectory reconstruction contains the assumption of diffusional motion, it is obvious that trajectories can be used to learn about molecular mobility on the nanometer scale. A detailed description will be given in the next subsection. It should be mentioned, however, that mobility information can be directly extracted from the position data. Here the position data are used to construct spatial image correlations that directly yield the desired molecular mobilities at nanometer accuracy (particle image correlation spectroscopy [PICS]; [95]). The advantage of correlation analysis is that it is very robust, and the accuracy of the mobility parameter extracted is clearly defined by statistics. The disadvantage clearly is that it is impossible to trace back to individual events or individual molecules as sometimes desired, as described later.

2.4. Learning from Trajectories

Although there is currently an intense discussion on the movements of membrane lipids over molecular distances [96–98], Brownian motion is considered as the appropriate model

when studying movements over length scales of tens of nanometers. We summarize here a few essentials of diffusion models; a more detailed overview can be found in Ref. 99.

A Brownian walker starting at time $t = 0$ at position $\vec{x}_0$ will be found at a later time t within the interval $\left[\vec{x},\vec{x} + d\vec{x}\right]$ with a probability

$$p\left(\vec{x},t\right) dx = \frac{1}{\sqrt{\left(4\pi Dt\right)^d}} \exp\left(-\frac{\left(\vec{x} - \vec{x}_0\right)^2}{4Dt}\right) d\vec{x}$$

where D denotes the diffusion coefficient and d the number of dimensions. Because diffusion has no preference for a particular direction, the average position of the tracer at any instant of time will be its starting position, $\langle \vec{x}\left(t\right)\rangle = \int \vec{x} p\left(\vec{x},t\right) d\vec{x} = \vec{x}_0$. Concurrently, it will be localized at a characteristic distance away from the starting point $\left\langle x^2\left(t\right)\right\rangle = \int \left(\vec{x} - \vec{x}_0\right)^2 p\left(\vec{x},t\right) d\vec{x} = 2dDt$. The distance $\left\langle x^2\left(t\right)\right\rangle$ is frequently termed mean square displacement (msd); it increases linearly with time, with the slope specifying the diffusion coefficient. It is further worthwhile to inspect the distribution $p\left(\vec{x},t\right) d\vec{x}$ more closely. For convenience, let us set $\vec{x}_0 = \vec{0}$. In the case of two-dimensional diffusion, the cumulative density function

$$\mathrm{cdf}(r^2,t) = \int_0^{r^2} p(\rho^2,t) d\rho^2$$

is given by

$$\mathrm{cdf}(r^2,t) = 1 - \exp\left(-\frac{r^2}{4Dt}\right)$$

with r denoting the 2D distance; note that this simple monoexponential expression is only valid for 2D diffusion.

Experimental data, however, contain localization errors, which have to be accounted for in the analysis. Localization errors can be well characterized using immobilized particles, and typically follow a Gaussian distribution

$$p_{err}\left(\vec{x}_{err}\right) d\vec{x}_{err} = \frac{1}{\sqrt{2\pi\sigma_{xy}^2}} \exp\left(-\frac{x_{err}^2}{2\sigma_{xy}^2}\right) d\vec{x}_{err}$$

Since the measured displacement is given by $\vec{x}_{\mathrm{exp}} = \vec{x} + 2\vec{x}_{err}$, the experimentally accessible probability distribution is a convolution of $p\left(\vec{x},t\right)$ and $p_{err}\left(\vec{x}_{err}\right)$, yielding

$$p\left(\vec{x},t\right) dx = \frac{1}{\sqrt{\left(4\pi Dt + 4\sigma_{xy}^2\right)^d}} \exp\left(-\frac{x^2}{4Dt + 4\sigma_{xy}^2}\right) d\vec{x}$$

For 2D diffusion, the cumulative density function changes to

$$\mathrm{cdf}(r^2,t) = 1 - \exp\left(-\frac{r^2}{4Dt + 4\sigma_{xy}^2}\right)$$

and the mean square displacement to $\left\langle x^2\left(t\right)\right\rangle = 4Dt + 4\sigma_{xy}^2$.

If the traced molecules follow free Brownian motion, tracking data may be used to study the diffusion coefficient under various conditions. Already 100 years ago, Einstein derived the famous fluctuation-dissipation theorem $D = k_{\mathrm{B}}T/\gamma$, with k_BT the Boltzmann energy and γ the Stokes friction coefficient; for a sphere of radius R moving in a fluid of viscosity η,

the mobility is characterized by $D = k_B T/6\pi\eta R$. Diffusion in a membrane, however, turned out to be more difficult to address. The seminal work by Saffman and Delbruck in 1975 found a logarithmic dependence of the diffusion coefficient on the radius of a cylindrical membrane protein [100]. Hughes et al. provided an extension for larger drag coefficients and concomitantly larger objects [101,102]; an approximation of the Hughes formula can be found in Ref. 103. In contrast, recent experimental data show strong deviations from the hydrodynamic models and indicate a Stokes-Einstein-like $1/R$-dependence of the diffusion coefficient [104].

Most researchers, however, have attempted to use single-molecule trajectories for identifying deviations from free Brownian motion. If the length of the observed trajectories exceeds hundreds of observations—for example, in single-particle tracking experiments—a detailed investigation at the level of a single trajectory is possible [105,106]. However, the lengths of single-molecule trajectories are limited by photobleaching to a couple of tens of observations [62], rendering such detailed analysis impracticable. We restrict our discussion here to approaches that average over multiple single-molecule trajectories. A more detailed discussion of diffusion analysis can be found in Ref. 107.

For example, multiple mobile fractions can be discriminated by analyzing the step-size distribution [32]. A mixture of two different fractions α and $(1 - \alpha)$ with mobility D_1 and D_2, respectively, can be identified as different exponential components in the cumulative density function

$$\mathrm{cdf} = 1 - \alpha \ \exp\left(-\frac{r^2}{4D_1 t}\right) - (1-\alpha) \ \exp\left(-\frac{r^2}{4D_2 t}\right)$$

The strategy has been successfully applied to identify subfractions of distinct mobility in model systems [32,38] and living cells [47].

Frequently, the diffusion of membrane proteins or lipids has been found to deviate from free Brownian motion and to be better described by anomalous subdiffusion, where the msd dependence on the time is characterized by a sublinear increase, $\mathrm{msd} \propto t^{\alpha}$, with $\alpha < 1$ the anomalous diffusion exponent [49,108–110]; in other words, the apparent diffusion coefficient appears to decrease with increasing time according to $D_{\mathrm{app}} = \mathrm{msd}/(4t) \propto t^{\alpha-1}$. Anomalous subdiffusion leads to an improved screening of the local environment and may therefore represent an important mechanism for enhancing the binding probability of the biomolecule to a nearby target [111]. Multiple studies have addressed potential sources of anomalous diffusion on cell membranes via Monte Carlo simulations [13,112–116]. In particular, fixed obstacles at concentrations close to the percolation threshold lead to a pronounced anomalous subdiffusion [13]. However, anomalous subdiffusion may also be misinferred by disregarding or incorrectly accounting for the finite localization precision [117]. In the following, we discuss the dependence of the mean-square displacement on time for different matrix geometries.

The confined diffusion of plasma membrane proteins or lipids within domains [8,18,40,42, 46,53,118] can be regarded as a specific case of subdiffusion. Analytical treatments have been provided for certain shapes of the confinement zones, thereby enabling quantitative estimates of the confinement size and the characteristic mobilities. For example, the diffusion of a tracer with mobility D_{micro} inside an impermeable circular or square corral has been described analytically [18,116]. For short time-lags, the function can be approximated by free diffusion, $\mathrm{msd}(t \to 0) \approx 4D_{\mathrm{micro}}t$; in the limit of long time-lags a constant offset is reached at the radius of gyration, which is $L^2/3$ for a square of length L and is R^2 for a circle of radius R [116].

We recently generalized the analytical treatment to the case of a meshwork of periodic permeable corrals, so that the tracer can escape into the adjacent compartment, performing a type of motion referred to as hop diffusion [42]. In this case, a transition between rapid microscopic diffusion within the domains and slow macroscopic diffusion from domain to domain can be observed. Figure 2.4 shows the time dependence of both msd (Figure 2.4A) and D_{app} (Figure 2.4B), the latter in a double-logarithmic plot. In that representation,

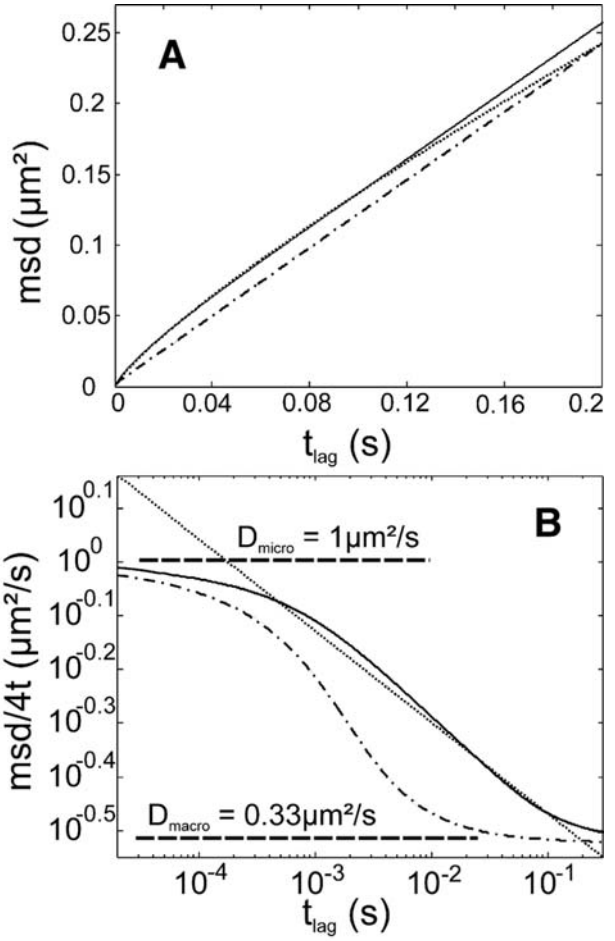

Figure 2.4. Effect of different geometries on the time dependence of the mean square displacement (msd) [107]. Hop diffusion in a meshwork of squares yields an apparent anomalous subdiffusion, in particular when the measurement is performed within a small time window. Hop diffusion was simulated with a mesh-size of $L = 0.1$ μm, a microscopic mobility of 1 μm^2/sec, and $\hat{\tau} = 3.33$ (*dot-dashed line*). **A.** The msd as a function of t_{lag}. **B.** The apparent diffusion constant $D_{\text{app}} = \text{msd}/(4t_{\text{lag}})$ versus t_{lag} on a log scale. In panel B the transition between the microscopic mobility on the left and the macroscopic mobility on the right is clearly visible. The transition region yields a rather straight line within a time window of about one order of magnitude. The effect smears out in the case of a distribution of confinement sizes, as shown in a simulation of equal contributions from $L = 0.1$, 0.2, and 0.5 μm (*solid line*). The curve can be well approximated by anomalous subdiffusion with msd $\propto t_{\text{lag}}^{0.83}$ over a time window of two orders of magnitude (*dotted line*). (Reprinted from Wieser and Schütz [107].)

anomalous subdiffusion would yield a linear decrease of $\log(D_{\text{app}})$ with $\log(t)$. Hop diffusion shows a different behavior, with the two mobility regimes being clearly discriminated as two plateaus for D_{micro} and D_{macro}, separated by a rather linear transition region. However, to identify both plateaus a time window of about four orders of magnitude is required, which is typically not available from experimental data. Within experimentally reasonable time windows of about one order of magnitude, the curves can be also well approximated by standard anomalous subdiffusion, making it difficult to distinguish those models. The linear transition region gets even larger if a natural variation in the domain sizes occurs. Figure 2.4 shows a scenario assuming equal contributions from domains with size 100, 200, and 500 nm. In this case, a time window of two orders of magnitude can be well fitted by msd $\propto t^{\alpha}$; researchers would not doubt to ascribe such results to anomalous subdiffusion.

Many more 2D diffusion models can be constructed that yield mutually similar or identical results. For example, a well-known model for organelle transport assumes the diffusion of the tracer in an impermeable mobile domain [119]. This model may well be applicable for describing protein mobility in cell membranes, in particular in view of recent studies indicating the existence of protein islands in the cellular plasma membrane [120]. However, when analyzing msd versus t, a moving-domain model yields the same result as a hop diffusion model, rendering the two cases indistinguishable. It should be emphasized that such ambiguities require cautious application of diffusion analysis based on msd, in particular when different diffusion models are to be distinguished.

Measurements of the lateral diffusion typically assume that the biomolecule moves in a flat plane. Yet, undulations or fluctuations of the membrane on a length scale close to the localization precision absolutely can be expected. In this case, the projection of the movement onto the focal plane will be observed. Ruffled surfaces or thermal membrane fluctuations will essentially reduce the diffusion constant [121–123]; more dramatic effects may be expected when the biomolecule enters highly curved 3D structures. We recently calculated and measured the one-dimensional mobility of membrane proteins diffusing along the circumference of tunneling nanotubules (TNTs) [44], cylindrical structures with a radius $R \approx 130$ nm that interconnect different cells for membrane and organelle exchange [124]. Since the molecules are tied to the cylindrical surface of the TNT, the msd for transverse motion saturates at R^2 for long time-lags. For short time-lags, the mobility can be approximated by msd $\approx D_{\perp} t_{\text{lag}}$, concomitant with a reduction in the apparent mobility by a factor of two.

Finally, the motion of the tracer during its illumination will change the recorded displacements to reduced values [107]. This effect is present for a freely diffusing molecule [125] and becomes dramatic for confined molecules [42,110,126].

2.5. Application 1—Synthetic Lipid Bilayers

The application of single-molecule microscopy to synthetic bilayers [29] was key for the development of single-molecule technology for biosciences and cell biology [127]. Similarly, synthetic bilayers are an excellent arena in which to understand the underlying properties of cellular membranes and as a substrate for bio-nanoscience applications: For both, the microscopic structure of mixed bilayers systems has been of prime scientific interest. When lipids of different phase transition temperature are mixed and the temperature lowered, demixing and macroscopic phase separation occurs [128]. Domain size and domain dynamics of such systems can be addressed by single-molecule methods. Labeling of a trace amount of lipids with a fluorescence marker allowed us directly to visualize the diffusional motion of lipids

in a supported membrane [32], in a free-standing membrane spanning a micron-sized hole [34], and in the membrane of giant unilamellar vesicles (GUVs) (S. Semrau and T. Schmidt, unpublished, 2007). The significant increase in mobility from $D = 4\ \mu m^2/sec$ in supported membranes to $D = 10–20\ \mu m^2/sec$ in free-standing membranes and GUVs clearly shows the influence of the membrane–substrate interaction on lipid mobility (Figure 2.6A). Depending on the preparation technique, this interaction can be quite inhomogeneous, leading to domains or diffusion-barrier formation on the hundred-nanometer length scale as resolved by single-molecule tracking experiments [32]. Whereas those domains, due to imperfections of bilayers formation even in unimolecular systems, are undisputed, the appearance of nanometric domains in more complicated mixed systems like the universal phosphocholine-sphingolipid-cholesterol 1:1:1 "raft" mixture close to the demixing point is still under investigation (Figure 2.5). This is because the lateral mobility of lipids in the liquid-ordered and liquid-disordered phases, respectively, is very similar and hence difficult to distinguish. Multiparameter single-molecule microscopy, however, might be able to solve the experimental problem. Dual-channel imaging with the fluorescence anisotropy as readout has been developed to address fast rotational motion [35] and fluorescence resonant energy transfer [129] in bilayers systems. As the rotational motion of lipids in the liquid-ordered state is significantly lower than in the liquid-disordered state, trajectory analysis as described in the last subsection combined with simultaneous analysis of the rotational mobility might give an indication of whether nanoscopic phase separation does occur. At least the macroscopic phase separation

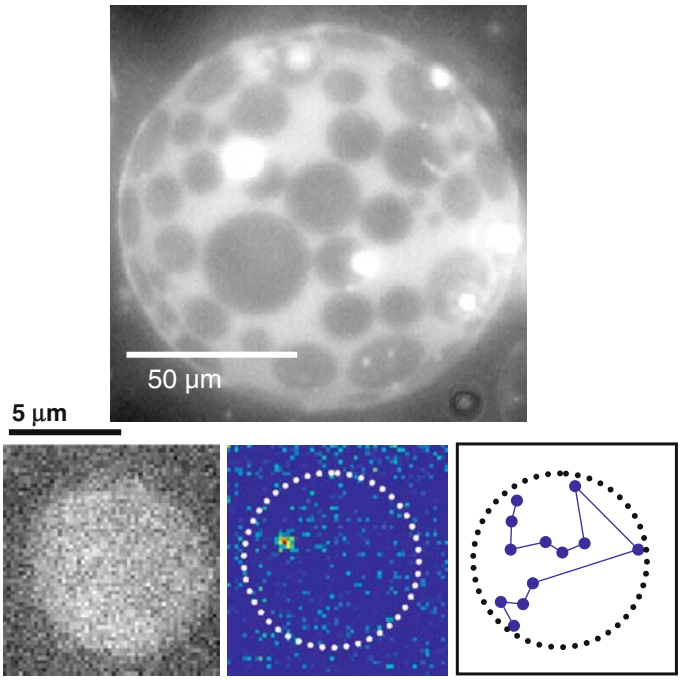

Figure 2.5. Individual lipids in a phase-separated giant unilamellar vesicle **(top)** were followed over time. Dual-color imaging was used to visualize the fluid domain in the green using a DiI stain **(bottom left)** and individual Cy5-labeled phospholipids **(bottom middle)** simultaneously. The lipid performed Brownian motion confined to the fluid-disordered domain. (S. Semrau, unpublished, 2008.)

far from the demixing point seen in GUVs did allow us to estimate the expected size of those nanodomains close to the demixing point. Analysis of the shape of macroscopic phase-separated 1:1:1 GUVs yields a line tension of 4 pN, which allowed us to estimate upper and lower limits for the size of phase-separated domains in the range of 10–30 nm [95]. This finding based on the mechanical properties of bilayers goes along with the lipid-shell models currently being discussed for cellular membranes [130].

A novel domain that comes into reach by single-molecule studies on bilayers systems is the analysis of mobility in complex and crowded environments [111,131]. The artificial environment of bilayers allows us precisely to adjust the amount of molecular players, including some that are attached to the membrane, and by that occupying space make it unavailable to other molecules. Such molecular crowding is believed to play an important role in cellular processes on membranes, in the cytosol, and in the nucleus, and is technically used for example, to enhance protein crystallization. Since part of the total volume is occupied by crowding agents, dynamic processes like signaling or random searching can be largely enhanced. Single-molecule microscopy does allow us now to directly follow individual players in, for example, a signaling pathway, and by such experiments we will be able to observe the influence of the crowding agent on the effectiveness and reliability of diffusion-controlled interactions. Similarly, groups are using membrane systems like GUVs for the construction of artificial biological systems [132], systems that at least in part mimic processes seen in nature.

As a conclusion to this subsection, we note that single-molecule microscopy has opened new opportunities for studies of artificial bilayer systems. Building on a vast amount of literature on the physical chemistry of monolayer and bilayers systems, the possibility to observe and follow an individual molecule within the bilayer or a vesicle as an artificial cell will spur novel and exciting research in a field localized among physics, material sciences, and cell biology [4].

2.6. Application 2—Live Cell Plasma Membrane

The successful utilization of single-molecule microscopy for the study of model membranes has yielded the promising perspective of a rather instantaneous application to living cells. However, the frequent occurrence of many species of endogenous fluorescent molecules inside cells has made such an application difficult. Cellular autofluorescence has been characterized in terms of spectral properties [133], lifetime [134], and spatial distribution [135]. In the visible regime, flavins [133] and lipofuscin [136] are currently regarded as the major source of endogenous fluorescence. Flavins are mainly located in mitochondria, whereas lipofuscins predominantly reside in lysosomes. In fluorescence images, both organelles appear as diffraction-limited spots randomly distributed in the cytoplasm of the cell. The high variability of the fluorescence intensity of such spots, even within one cell, makes unambiguous distinction between fluorophores and autofluorescence a challenging task.

In general, it turned out that the brightness of autofluorescent structures decreases with increasing wavelength, rendering red excitation beyond 600 nm the pragmatic choice [40,41]. However, frequently the biological problem defines both the cell type and the excitation color to use. For such cases, methods for the decomposition of optical signals originating from two spectrally distinct components may be used [137].

Having selected the proper dye, there are several ways for attaching it to the biomolecule of interest:

1. The purified or synthesized biomolecule is directly labeled covalently with a fluorescent marker and subsequently added to the living cell. This strategy has been applied for the study of small molecules like lipids [40] and for larger stable structures such as viruses [138]. In addition, exogenously applied lipid-anchored proteins were found to incorporate into the plasma membrane and acquire the correct signaling capacity [139].
2. The protein of interest is genetically fused to a fluorescent protein [140], a specific tag, or a protein that can be covalently labeled with an exogenously added dye (Snap-tag) [141]. In particular, since the spectroscopic properties of the available fluorescent protein mutants are inferior to those of many organic fluorophores [91], covalent labeling strategies have found widespread approval of the researchers.
3. Membrane proteins can be specifically labeled by fluorescent ligands such as Fab fragments [42, 43] or toxins [142].

Whereas specific monovalent labeling is rather straightforward for single-dye approaches, it represents a big challenge for SPT. Commonly, particles are coated with a mix of specific antibody and a blocking protein, typically bovine serum albumin (BSA). By reducing the amount of antibody, researchers attempt to reduce the likelihood of particles containing more than one accessible reactive group. As expected, the multivalency of the particle reduces the mobility of the tracer [19]. Indeed, results obtained by SPT can differ significantly from the undisturbed motion of the molecule of interest. In one study, residual cross-linking of the diffusing probe was found to reduce the diffusion coefficients significantly when compared to data obtained from tracking the same probe labeled via a fluorescent antibody [52]. A different study reported the alteration of the diffusion behavior from free diffusion to anomalous subdiffusion on labeling with quantum dots [143]. With the development of small passivated quantum dots, however, monovalency of a particle may indeed come into reach [144].

Most single-molecule studies on the plasma membrane have aimed at the identification of confinements to the free diffusion of the tracer. In particular, when molecules undergo direct or indirect interactions with the membrane skeleton, the diffusional motion becomes transiently restricted to membrane domains. Such confinements are highly relevant for theoretical modeling because they affect the interaction probability between arbitrary molecules. These confinement zones were postulated long before they were actually seen [145]. The first evidence for the existence of structural domains within the plasma membrane of cells came from biochemical extraction of the membrane together with subsequent sucrose density gradient centrifugation, which made it possible qualitatively to distinguish a distinct part of the plasma membrane that is not soluble in mild detergent [146]. Careful investigation of such detergent-resistant membranes (DRMs) further yielded their protein content, which was found to be consistently different from the remaining fractions of the membrane [147,148]. Of interest, DRMS were found to be enriched in proteins involved in signaling [149].

The physical origin and *in vivo* counterpart of DRMs are under debate. The detergent insolubility is most likely mediated by self-interaction between glycosphingolipids [15]. In addition, DRMs contain a distinct set of lipids [146], such as sphingolipids [150], fully saturated fatty acids [151], and cholesterol [146]. Detergent-resistant liposomes were found to be in liquid-ordered phase [15,152]. This ordered environment highly enhances the partitioning of proteins that are linked to saturated acyl chains, such as glycosylphosphatidylinositol (GPI)-anchored proteins or proteins acylated with myristate or palmitate [153,154]. Taken together, those studies were the experimental basis for the formulation of the "raft theory,"

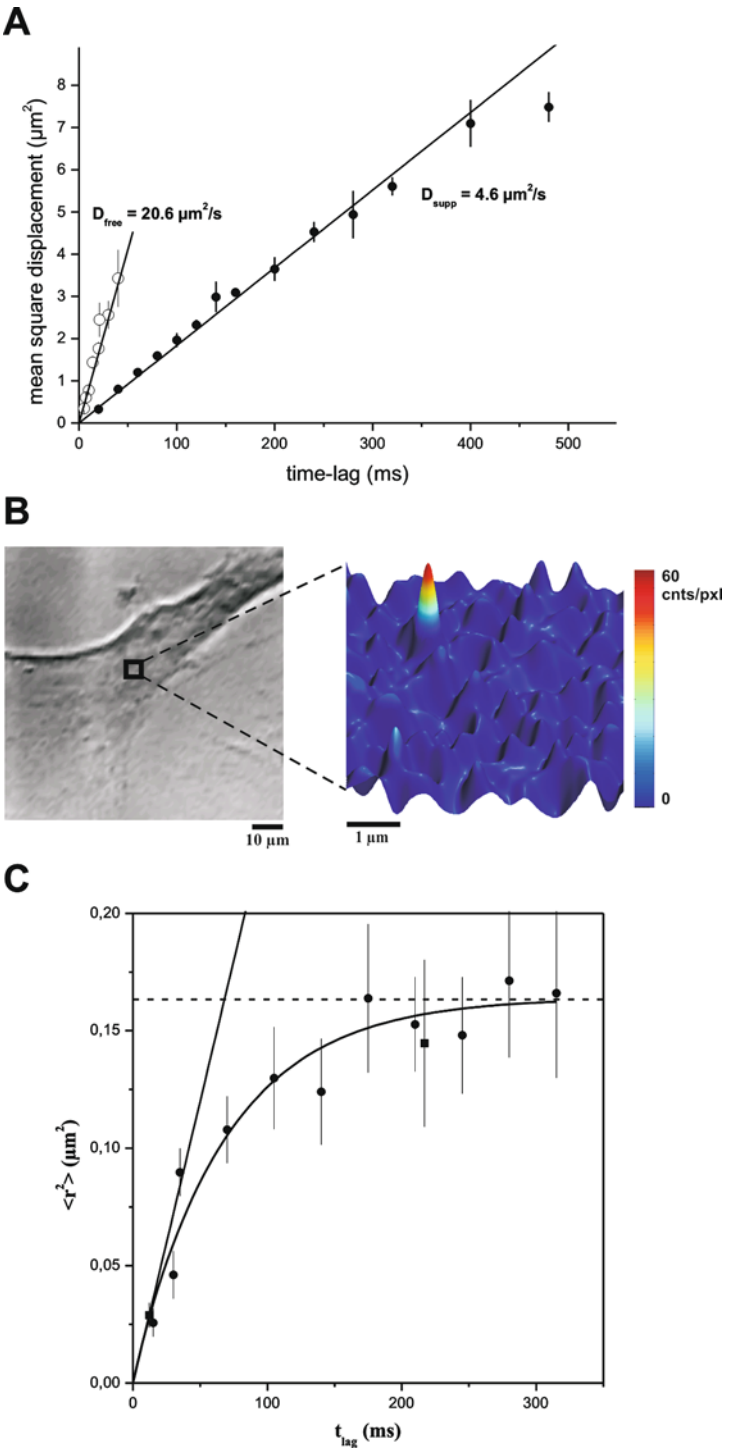

Figure 2.6. (continued)

in which the existence of stable platforms within the plasma membrane, membranes of organelles, and membranes of transport vesicles has been postulated [15].

Beside its initial importance for the discovery of plasma membrane domains, detergent extraction methods are still widely used to study the targeting of membrane proteins, either to rafts or to the remaining part of the plasma membrane. However, there are limitations to this method. First, artifacts due to relocalization of proteins during detergent extraction have been reported [155,156]. Second, a note of caution was recently raised against the structural interpretation of biochemical data by pointing out that rafts may be altered or even formed on detergent treatment [157]. Third, to avoid degradation processes, solubilization of cells is commonly performed at low temperatures, which most likely has an effect on the phase state of the domain and might alter its physical properties [158,159]. Note that analysis of the solubility in detergent reveals no information on the actual size, shape, and dynamical properties of domains.

SPT has been developed as a technique to study the compartmentalization of cell surfaces [8,17,18,94,160,161]. Restrictions to the lateral mobility have been observed for proteins such as Band 3 [162], E-cadherin [12], neural cell adhesion molecule (NCAM) [163], the transferrin receptor [164], and even for phospholipids themselves [8]. In most of those studies, the structural origin of the constraint was found to be the membrane-skeleton meshwork. Recent studies identified details in the molecular mechanism for transient immobilization of clustered GPI-anchored proteins [9,10,165].

In addition, lipid rafts have been reinterpreted in view of single-particle tracking data that revealed hop diffusion of essentially all investigated membrane probes [5]. The results of those studies provoked the current view of lipid rafts as highly dynamic objects, which are expected to mediate the coupling of the cortical actin meshwork to the exoplasmic membrane leaflet [166]. We and others therefore attempted to confirm or correct this model, based on the less invasive single-molecule imaging approach.

By pushing instrumentation to the theoretical limits, we were able to measure the mobility of single GPI-anchored proteins in the live cell plasma membrane at a resolution of $\sim$20 nm in space and <1 ms in time. For the raft protein CD59 we found no indication for hop diffusion and, as consequence, no indication for the presence of short-lived lipid rafts [42]. We further addressed this aspect by analyzing the mobility of the same GPI protein diffusing on the surface of cellular nanotubules— recently discovered thin structures that

Figure 2.6. A. Comparison of the diffusion in a free-standing ($\bigcirc$) and supported membrane ($\bullet$) [34]. For both, the mean square displacement increases linearly with time lag, yielding diffusion constants of $D_{\text{free}} = 20.6 \pm 0.9\ \mu\text{m}^2/\text{secand}\ D_{\text{supp}} = 4.6 \pm 0.1\ \mu\text{m}^2/\text{sec}$, respectively. (Reprinted by permission from Sonnleitner et al. [34], copyright 1999 by the Biophysical Society.) **B.** Single-lipid imaging in the plasma membrane of a human smooth muscle cell [40]. On the left, the cell is shown in a transmission light image at 40× magnification. The square at the center indicates the area selected for fluorescence imaging (*right*). The cell was pretreated with Cy5-labeled dioleylphosphatidylethanolamine (DOPE-Cy5) so that a low concentration of the fluorescent lipid was incorporated into the plasma membrane. The clearly resolved peak corresponds to a single DOPE-Cy5 molecule. (Reprinted from Schütz et al. [40].) **C.** Mobility of single Cy5-labeled dimyristoylphosphatidylethanolamine (DMPE-Cy5) molecules in the plasma membrane of living human smooth muscle cells [40]. The mean square displacement $\left\langle r^2 \right\rangle$ as a function of the time-lag shows saturation for $t_{\text{lag}} > 100$ ms. From a fit to the model of restricted diffusion, the diffusion constant within a membrane microdomain, $D = 0.6 \pm 0.04\ \mu\text{m}^2/\text{sec}$ (*solid line*), and the domain size of 700 ± 20 nm (*dashed line*) were determined. (Reprinted from Schütz et al. [40].)

connect different cells. The high resolution in space and time allowed us to follow the diffusion process not only in the longitudinal direction, but also along the circumference. We found perfectly isotropic mobility, in line with our previous observation that the anisotropic membrane skeleton does not impose a meshwork of periodic boundaries to the diffusion of exoplasmic plasma membrane constituents [44].

Although the general mechanism of hop diffusion remains controversial, there is no doubt that numerous membrane constituents become trapped in specific cell surface regions. Confinements to immobile domains were indeed reported for a fully saturated lipid in a human smooth muscle cell line [40] (Figure 2.6B and C), the membrane anchor of Ras- and Src-family proteins [45–47], a G protein–coupled receptor [57], and hemagglutinin from the influenza virus [55]. Whether these structures correspond in general to lipid rafts, represent a subclass of lipid rafts, or can be considered as different organization units remains to be solved.

Acknowledgments

This work was supported by the Austrian Science Fund (FWF project Y250-B10) and the GEN-AU project of the Austrian Federal Ministry for Science and Research (GJS). This work is part of the research program of the Stichting voor Fundamenteel Onderzoek der Materie (FOM), which is financially supported by the Nederlandse Organisatie voor Wetenschappelijk Onderzoek (NWO) (TS).

References

1. Singer, S. J., and G. L. Nicolson. 1972. The fluid mosaic model of the structure of cell membranes. Science 175:720–731.
2. Lipowsky, R., and E. Sackmann, editors. 1995. Structure and dynamics of membranes. Amsterdam: Elsevier.
3. Vereb, G., J. Szollosi, J. Matko, P. Nagy, T. Farkas, L. Vigh, L. Matyus, T. A. Waldmann, and S. Damjanovich. 2003. Dynamic, yet structured: the cell membrane three decades after the Singer-Nicolson model. Proc Natl Acad Sci USA 100:8053–8058.
4. Jacobson, K., O. G. Mouritsen, and R. G. Anderson. 2007. Lipid rafts: at a crossroad between cell biology and physics. Nat Cell Biol 9:7–14.
5. Kusumi, A., C. Nakada, K. Ritchie, K. Murase, K. Suzuki, H. Murakoshi, R. S. Kasai, J. Kondo, and T. Fujiwara. 2005. Paradigm shift of the plasma membrane concept from the two-dimensional continuum fluid to the partitioned fluid: high-speed single-molecule tracking of membrane molecules. Annu Rev Biophys Biomol Struct 34:351–378.
6. Lenne, P. F., L. Wawrezinieck, F. Conchonaud, O. Wurtz, A. Boned, X. J. Guo, H. Rigneault, H. T. He, and D. Marguet. 2006. Dynamic molecular confinement in the plasma membrane by microdomains and the cytoskeleton meshwork. EMBO J 25:3245–3256.
7. Anderson, R. G., and K. Jacobson. 2002. A role for lipid shells in targeting proteins to caveolae, rafts, and other lipid domains. Science 296:1821–1825.
8. Fujiwara, T., K. Ritchie, H. Murakoshi, K. Jacobson, and A. Kusumi. 2002. Phospholipids undergo hop diffusion in compartmentalized cell membrane. J Cell Biol 157:1071–1081.
9. Chen, Y., W. R. Thelin, B. Yang, S. L. Milgram, and K. Jacobson. 2006. Transient anchorage of cross-linked glycosyl-phosphatidylinositol-anchored proteins depends on cholesterol, Src family kinases, caveolin, and phosphoinositides. J Cell Biol 175:169–178.
10. Suzuki, K. G., T. K. Fujiwara, F. Sanematsu, R. Iino, M. Edidin, and A. Kusumi. 2007. GPI-anchored receptor clusters transiently recruit Lyn and G{alpha} for temporary cluster immobilization and Lyn activation: single-molecule tracking study 1. J Cell Biol 177: 717–730.
11. Demond, A. L., K. D. Mossman, T. Starr, M. L. Dustin, and J. T. Groves. 2008. T cell receptor microcluster transport through molecular mazes reveals mechanism of translocation. Biophys J 94:3286–3292.

12. Sako, Y., A. Nagafuchi, S. Tsukita, M. Takeichi, and A. Kusumi. 1998. Cytoplasmic regulation of the movement of E-cadherin on the free cell surface as studied by optical tweezers and single particle tracking: corralling and tethering by the membrane skeleton. J Cell Biol 140:1227–1240.
13. Saxton, M. J. 1994. Anomalous diffusion due to obstacles: a Monte Carlo study. Biophys J 66:394–401.
14. Marguet, D., P. F. Lenne, H. Rigneault, and H. T. He. 2006. Dynamics in the plasma membrane: how to combine fluidity and order. EMBO J 25:3446–3457.
15. Simons, K., and E. Ikonen. 1997. Functional rafts in cell membranes. Nature 387:569–572.
16. Barak, L. S., and W. W. Webb. 1981. Fluorescent low density lipoprotein for observation of dynamics of individual receptor complexes on cultured human fibroblasts. J Cell Biol 90:595–604.
17. Kusumi, A., Y. Sako, and M. Yamamoto. 1993. Confined lateral diffusion of membrane receptors as studied by single particle tracking (nanovid microscopy). Effects of calcium-induced differentiation in cultured epithelial cells. Biophys J 65:2021–2040.
18. Saxton, M. J., and K. Jacobson. 1997. Single-particle tracking: applications to membrane dynamics. Annu Rev Biophys Biomol Struct 26:373–399.
19. Lee, G. M., A. Ishihara, and K. A. Jacobson. 1991. Direct observation of Brownian motion of lipids in a membrane. Proc Natl Acad Sci USA 88:6274–6278.
20. Wilson, K. M., I. E. Morrison, P. R. Smith, N. Fernandez, and R. J. Cherry. 1996. Single particle tracking of cell-surface HLA-DR molecules using R-phycoerythrin labeled monoclonal antibodies and fluorescence digital imaging. J Cell Sci 109 (Pt 8):2101–2109.
21. Kao, H. P., and A. S. Verkman. 1994. Tracking of single fluorescent particles in three dimensions: use of cylindrical optics to encode particle position. Biophys J 67:1291–1300.
22. Felsenfeld, D. P., D. Choquet, and M. P. Sheetz. 1996. Ligand binding regulates the directed movement of beta1 integrins on fibroblasts. Nature 383:438–440.
23. Anderson, C. M., G. N. Georgiou, I. E. Morrison, G. V. Stevenson, and R. J. Cherry. 1992. Tracking of cell surface receptors by fluorescence digital imaging microscopy using a charge-coupled device camera. Low-density lipoprotein and influenza virus receptor mobility at 4 degrees C. J Cell Sci 101(Pt 2): 415–425.
24. Fein, M., J. Unkeless, F. Y. Chuang, M. Sassaroli, R. da Costa, H. Vaananen, and J. Eisinger. 1993. Lateral mobility of lipid analogues and GPI-anchored proteins in supported bilayers determined by fluorescent bead tracking. J Membr Biol 135:83–92.
25. Geerts, H., M. De Brabander, R. Nuydens, S. Geuens, M. Moeremans, J. De Mey, and P. Hollenbeck. 1987. Nanovid tracking: a new automatic method for the study of mobility in living cells based on colloidal gold and video microscopy. Biophys J 52: 775–782.
26. Thompson, R. E., D. R. Larson, and W. W. Webb. 2002. Precise nanometer localization analysis for individual fluorescent probes. Biophys J 82:2775–2783.
27. Kuno, M., D. P. Fromm, H. F. Hamann, A. Gallagher, and D. J. Nesbitt. 1999. Nonexponential "blinking" kinetics of single CdSe quantum dots: a universal power law behavior. J Chem Phys 112:3117–3120.
28. Schmidt, T., G. J. Schütz, W. Baumgartner, H. J. Gruber, and H. Schindler. 1995. Characterization of photophysics and mobility of single molecules in a fluid lipid membrane. J Phys Chem 99: 17662–17668.
29. Schmidt, T., G. J. Schütz, W. Baumgartner, H. J. Gruber, and H. Schindler. 1996. Imaging of single molecule diffusion. Proc Natl Acad Sci USA 93:2926–2929.
30. Funatsu, T., Y. Harada, M. Tokunaga, K. Saito, and T. Yanagida. 1995. Imaging of single fluorescent molecules and individual ATP turnovers by single myosin molecules in aqueous-solution. Nature 374:555–559.
31. Sase, I., H. Miyata, J. E. Corrie, J. S. Craik, and K. Kinosita, Jr. 1995. Real time imaging of single fluorophores on moving actin with an epifluorescence microscope. Biophys J 69: 323–328.
32. Schütz, G. J., H. Schindler, and T. Schmidt. 1997. Single-molecule microscopy on model membranes reveals anomalous diffusion. Biophys J 73:1073–1080.
33. Schütz, G. J., W. Trabesinger, and T. Schmidt. 1998. Direct observation of ligand colocalization on individual receptor molecules. Biophys J 74:2223–2226.
34. Sonnleitner, A., G. J. Schutz, and T. Schmidt. 1999. Free Brownian motion of individual lipid molecules in biomembranes. Biophys J 77:2638–2642.
35. Harms, G. S., M. Sonnleitner, G. J. Schütz, H. J. Gruber, and T. Schmidt. 1999. Single-molecule anisotropy imaging. Biophys J 77:2864–2870.
36. Ke, P. C., and C. A. Naumann. 2001. Hindered diffusion in polymer-tethered phosopholipid monolayers at the air–water interface: a single molecule fluorescence imaging study. Langmuir 17:5076–5081.
37. Ke, P. C., and C. A. Naumann. 2001. Single molecule fluorescence imaging of phospholipid monolayers at the air–water interface. Langmuir 17:3727–3733.

38. Deverall, M. A., E. Gindl, E. K. Sinner, H. Besir, J. Ruehe, M. J. Saxton, and C. A. Naumann. 2005. Membrane lateral mobility obstructed by polymer-tethered lipids studied at the single molecule level. Biophys J 88: 1875–1886.
39. Kiessling, V., J. M. Crane, and L. K. Tamm. 2006. Transbilayer effects of raft-like lipid domains in asymmetric planar bilayers measured by single molecule tracking. Biophys J 91:3313–3326.
40. Schütz, G. J., G. Kada, V. P. Pastushenko, and H. Schindler. 2000. Properties of lipid microdomains in a muscle cell membrane visualized by single molecule microscopy. EMBO J 19:892–901.
41. Schütz, G. J., V. P. Pastushenko, H. J. Gruber, H.-G. Knaus, B. Pragl, and H. Schindler. 2000. 3D Imaging of individual ion channels in live cells at 40 nm resolution. Single Mol. 1:25–31.
42. Wieser, S., M. Moertelmaier, E. Fuertbauer, H. Stockinger, and G. J. Schutz. 2007. (Un)Confined diffusion of CD59 in the plasma membrane determined by high-resolution single molecule microscopy. Biophys J 92: 3719–3728.
43. Drbal, K., M. Moertelmaier, C. Holzhauser, A. Muhammad, E. Fuertbauer, S. Howorka, M. Hinterberger, H. Stockinger, and G. J. Schutz. 2007. Single-molecule microscopy reveals heterogeneous dynamics of lipid raft components upon TCR engagement. Int Immunol 19:675–684.
44. Wieser, S., G. J. Schutz, M. E. Cooper, and H. Stockinger. 2007. Single molecule diffusion analysis on cellular nanotubules: implications on plasma membrane structure below the diffraction limit. Appl Phys Lett 91:233901.
45. Lommerse, P. H., K. Vastenhoud, N. J. Pirinen, A. I. Magee, H. P. Spaink, and T. Schmidt. 2006. Single-molecule diffusion reveals similar mobility for the Lck, H-ras, and K-ras membrane anchors. Biophys J 91:1090–1097.
46. Lommerse, P. H., B. E. Snaar-Jagalska, H. P. Spaink, and T. Schmidt. 2005. Single-molecule diffusion measurements of H-Ras at the plasma membrane of live cells reveal microdomain localization upon activation. J Cell Sci 118:1799–1809.
47. Lommerse, P. H., G. A. Blab, L. Cognet, G. S. Harms, B. E. Snaar-Jagalska, H. P. Spaink, and T. Schmidt. 2004. Single-molecule imaging of the H-Ras membrane-anchor reveals domains in the cytoplasmic leaflet of the cell membrane. Biophys J 86:609–616.
48. Harms, G. S., L. Cognet, P. H. Lommerse, G. A. Blab, H. Kahr, R. Gamsjager, H. P. Spaink, N. M. Soldatov, C. Romanin, and T. Schmidt. 2001. Single-molecule imaging of l-type Ca(2+) channels in live cells. Biophys J 81:2639–2646.
49. Vrljic, M., S. Y. Nishimura, S. Brasselet, W. E. Moerner, and H. M. McConnell. 2002. Translational diffusion of individual class II MHC membrane proteins in cells. Biophys J 83:2681–2692.
50. Vrljic, M., S. Y. Nishimura, W. E. Moerner, and H. M. McConnell. 2005. Cholesterol depletion suppresses the translational diffusion of class II major histocompatibility complex proteins in the plasma membrane. Biophys J 88:334–347.
51. Nishimura, S. Y., M. Vrljic, L. O. Klein, H. M. McConnell, and W. E. Moerner. 2006. Cholesterol depletion induces solid-like regions in the plasma membrane. Biophys J 90: 927–938.
52. Umemura, Y. M., M. Vrljic, S. Y. Nishimura, T. K. Fujiwara, K. G. Suzuki, and A. Kusumi. 2008. Both MHC class II and its GPI-anchored form undergo hop diffusion as observed by single-molecule tracking. Biophys J 95:435–450.
53. Murase, K., T. Fujiwara, Y. Umemura, K. Suzuki, R. Iino, H. Yamashita, M. Saito, H. Murakoshi, K. Ritchie, and A. Kusumi. 2004. Ultrafine membrane compartments for molecular diffusion as revealed by single molecule techniques. Biophys J 86:4075–4093.
54. Douglass, A. D., and R. D. Vale. 2005. Single-molecule microscopy reveals plasma membrane microdomains created by protein-protein networks that exclude or trap signaling molecules in T cells. Cell 121: 937–950.
55. Hess, S. T., T. J. Gould, M. V. Gudheti, S. A. Maas, K. D. Mills, and J. Zimmerberg. 2007. Dynamic clustered distribution of hemagglutinin resolved at 40 nm in living cell membranes discriminates between raft theories. Proc Natl Acad Sci USA 104:17370–17375.
56. Manley, S., J. M. Gillette, G. H. Patterson, H. Shroff, H. F. Hess, E. Betzig, and J. Lippincott-Schwartz. 2008. High-density mapping of single-molecule trajectories with photoactivated localization microscopy. Nat Methods 5:155–157.
57. Jacquier, V., M. Prummer, J. M. Segura, H. Pick, and H. Vogel. 2006. Visualizing odorant receptor trafficking in living cells down to the single-molecule level. Proc Natl Acad Sci USA 103:14325–14330.
58. James, J. R., S. S. White, R. W. Clarke, A. M. Johansen, P. D. Dunne, D. L. Sleep, W. J. Fitzgerald, S. J. Davis, and D. Klenerman. 2007. Single-molecule level analysis of the subunit composition of the T cell receptor on live T cells. Proc Natl Acad Sci USA 104:17662–17667.

59. Morimatsu, M., H. Takagi, K. G. Ota, R. Iwamoto, T. Yanagida, and Y. Sako. 2007. Multiple-state reactions between the epidermal growth factor receptor and Grb2 as observed by using single-molecule analysis. Proc Natl Acad Sci USA 104:18013–18018.
60. Sako, Y., S. Minoghchi, and T. Yanagida. 2000. Single-molecule imaging of EGFR signalling on the surface of living cells. Nat Cell Biol 2:168–172.
61. Ueda, M., Y. Sako, T. Tanaka, P. Devreotes, and T. Yanagida. 2001. Single-molecule analysis of chemotactic signaling in *Dictyostelium* cells. Science 294:864–867.
62. Füreder-Kitzmüller, E., J. Hesse, A. Ebner, H. J. Gruber, and G. J. Schütz. 2005. Non-exponential bleaching of single bioconjugated Cy5 molecules. Chem Phys Lett 404:13–18.
63. Hecht, E. 1987. Optics. Reading, MA: Addison-Wesley.
64. Enderlein, J., E. Toprak, and P. R. Selvin. 2006. Polarization effect on position accuracy of fluorophore localization. Opt Express 14:8111–8120.
65. Pohl, D. W., W. Denk, and M. Lanz. 1984. Optical stethoscopy: image recording with resolution λ/20. Appl Phys Lett 44:651–653.
66. Betzig, E., and J. K. Trautman. 1992. Near-field optics: microscopy, spectroscopy, and surface modification beyond the diffraction limit. Science 257:189–195.
67. Denk, W., J. H. Strickler, and W. W. Webb. 1990. Two-photon laser scanning fluorescence microscopy. Science 248:73–76.
68. Klar, T. A., S. Jakobs, M. Dyba, A. Egner, and S. W. Hell. 2000. Fluorescence microscopy with diffraction resolution barrier broken by stimulated emission. Proc Natl Acad Sci USA 97:8206–8210.
69. Pawley, J. B., editor. 1995. Handbook of biological confocal microscopy. New York: Plenum Press.
70. Gustafsson, M. G. 2005. Nonlinear structured-illumination microscopy: wide-field fluorescence imaging with theoretically unlimited resolution. Proc Natl Acad Sci USA 102:13081–13086.
71. Heintzmann, R., T. M. Jovin, and C. Cremer. 2002. Saturated patterned excitation microscopy—a concept for optical resolution improvement. J Opt Soc Am A – Opt Image Sci Vis 19:1599–1609.
72. Hell, S. W. 2007. Far-field optical nanoscopy. Science 316:1153–1158.
73. Betzig, E. 1995. Proposed method for molecular optical imaging. Opt Lett 20:237–239.
74. Bobroff, N. 1986. Position measurement with a resolution and noise-limited instrument. Rev Sci Instrum 57:1152–1157.
75. Yildiz, A., J. N. Forkey, S. A. McKinney, T. Ha, Y. E. Goldman, and P. R. Selvin. 2003. Myosin V walks hand-over-hand: single fluorophore imaging with 1.5-nm localization. Science 300:2061–2065.
76. Ober, R. J., S. Ram, and E. S. Ward. 2004. Localization accuracy in single-molecule microscopy. Biophys J 86:1185–1200.
77. Ha, T., T. Enderle, D. S. Chemla, and S. Weiss. 1996. Dual-molecule spectroscopy: molecular rulers for the study of biological macromolecules. IEEE J Sel Top Quant Electr 2: 1115–1128.
78. van Oijen, A. M., J. Kohler, J. Schmidt, M. Muller, and G. J. Brakenhoff. 1999. Far-field fluorescence microscopy beyond the diffraction limit. J Opt Soc Am A 16:909–915.
79. Trabesinger, W., G. J. Schütz, H. J. Gruber, H. Schindler, and T. Schmidt. 1999. Detection of individual oligonucleotide pairing by single-molecule microscopy. Anal Chem 71:279–283.
80. Trabesinger, W., B. Hecht, U. P. Wild, G. J. Schütz, H. Schindler, and T. Schmidt. 2001. Statistical analysis of single-molecule colocalization assays. Anal Chem 73:1100–1105.
81. Baumgartner, W., G. J. Schütz, J. Wiegand, N. Golenhofen, and D. Drenckhahn. 2003. Cadherin function probed by laser tweezer and single molecule fluorescence in vascular endothelial cells. J Cell Sci 116: 1001–1011.
82. Yildiz, A., M. Tomishige, R. D. Vale, and P. R. Selvin. 2004. Kinesin walks hand-over-hand. Science 303: 676–678.
83. Gordon, M. P., T. Ha, and P. R. Selvin. 2004. Single-molecule high-resolution imaging with photobleaching. Proc Natl Acad Sci USA 101:6462–6465.
84. Qu, X., D. Wu, L. Mets, and N. F. Scherer. 2004. Nanometer-localized multiple single-molecule fluorescence microscopy. Proc Natl Acad Sci USA 101:11298–11303.
85. Patterson, G. H., and J. Lippincott-Schwartz. 2002. A photoactivatable GFP for selective photolabeling of proteins and cells. Science 297:1873–1877.
86. Betzig, E., G. H. Patterson, R. Sougrat, O. W. Lindwasser, S. Olenych, J. S. Bonifacino, M. W. Davidson, J. Lippincott-Schwartz, and H. F. Hess. 2006. Imaging intracellular fluorescent proteins at nanometer resolution. Science 313:1642–1645.
87. Hess, S. T., T. P. Girirajan, and M. D. Mason. 2006. Ultra-high resolution imaging by fluorescence photoactivation localization microscopy. Biophys J 91:4258–4272.

88. Rust, M., M. Bates, and X. Zhuang. 2006. Sub-diffraction-limit imaging by stochastic optical reconstruction microscopy (STORM). Nat Methods 3:793–795.
89. Shroff, H., C. G. Galbraith, J. A. Galbraith, and E. Betzig. 2008. Live-cell photoactivated localization microscopy of nanoscale adhesion dynamics. Nat Methods 5:417–423.
90. Orrit, M., and J. Bernard. 1990. Single pentacene molecules detected by fluorescence excitation in a *p*-terphenyl crystal. Phys Rev Lett 65:2716–2719.
91. Harms, G. S., L. Cognet, P. H. Lommerse, G. A. Blab, and T. Schmidt. 2001. Autofluorescent proteins in single-molecule research: applications to live cell imaging microscopy. Biophys J 80:2396–2408.
92. Holtzer, L., T. Meckel, and T. Schmidt. 2007. Nanometric three-dimensional tracking of individual quantum dots in cells. Appl Phys Lett 90:053902.
93. Prabhat, P., Z. Gan, J. Chao, S. Ram, C. Vaccaro, S. Gibbons, R. J. Ober, and E. S. Ward. 2007. Elucidation of intracellular recycling pathways leading to exocytosis of the Fc receptor, FcRn, by using multifocal plane microscopy. Proc Natl Acad Sci USA 104:5889–5894.
94. Ghosh, R. N., and W. W. Webb. 1994. Automated detection and tracking of individual and clustered cell surface low density lipoprotein receptor molecules. Biophys J 66:1301–1318.
95. Semrau, S., and T. Schmidt. 2006. Particle image correlation spectroscopy (PICS) Retrieving nanometer-scale correlations from high-density single-molecule position data. Biophys J 92:613–621.
96. Falck, E., T. Rog, M. Karttunen, and I. Vattulainen. 2008. Lateral diffusion in lipid membranes through collective flows. J Am Chem Soc 130:44–45.
97. Almeida, P. F., W. L. Vaz, and T. E. Thompson. 2005. Lipid diffusion, free area, and molecular dynamics simulations. Biophys J 88:4434–4438.
98. Falck, E., M. Patra, M. Karttunen, M. T. Hyvonen, and I. Vattulainen. 2005. Response to comment by Almeida et al.: free area theories for lipid bilayers—predictive or not? Biophys J 89:745–752.
99. Berg, H. C. 1983. Random walks in biology. Princeton, New Jersey: Princeton University Press.
100. Saffman, P. G., and M. Delbruck. 1975. Brownian motion in biological membranes. Proc Natl Acad Sci USA 72:3111–3113.
101. Hughes, B. D., B. A. Pailthorpe, and L. R. White. 1981. The translational and rotational drag on a cylinder moving in a membrane. J. Fluid. Mech. 110:349–372.
102. Hughes, B. D., B. A. Pailthorpe, L. R. White, and W. H. Sawyer. 1982. Extraction of membrane microviscosity from translational and rotational diffusion coefficients. Biophys J 37:673–676.
103. Petrov, E. P., and P. Schwille. 2008. Translational diffusion in lipid membranes beyond the Saffman-Delbruck approximation. Biophys J 94:L41–43.
104. Gambin, Y., R. Lopez-Esparza, M. Reffay, E. Sierecki, N. S. Gov, M. Genest, R. S. Hodges, and W. Urbach. 2006. Lateral mobility of proteins in liquid membranes revisited. Proc Natl Acad Sci USA 103: 2098–2102.
105. Saxton, M. J. 1995. Single-particle tracking: effects of corrals. Biophys J 69:389–398.
106. Simson, R., E. D. Sheets, and K. Jacobson. 1995. Detection of temporary lateral confinement of membrane proteins using single-particle tracking analysis. Biophys J 69:989–993.
107. Wieser, S., and G. J. Schütz 2008. Tracking single molecules in the live cell plasma membrane—Do's and Don't's. Methods 46:131–140.
108. Feder, T. J., I. Brust-Mascher, J. P. Slattery, B. Baird, and W. W. Webb. 1996. Constrained diffusion or immobile fraction on cell surfaces: a new interpretation. Biophys J 70:2767–2773.
109. Smith, P. R., I. E. Morrison, K. M. Wilson, N. Fernandez, and R. J. Cherry. 1999. Anomalous diffusion of major histocompatibility complex class I molecules on HeLa cells determined by single particle tracking. Biophys J 76:3331–3344.
110. Ritchie, K., X. Y. Shan, J. Kondo, K. Iwasawa, T. Fujiwara, and A. Kusumi. 2005. Detection of non-Brownian diffusion in the cell membrane in single molecule tracking. Biophys J 88:2266–2277.
111. Guigas, G., and M. Weiss. 2007. Sampling the cell with anomalous diffusion—the discovery of slowness. Biophys J 94:90–94.
112. Nicolau, D. V., Jr., J. F. Hancock, and K. Burrage. 2007. Sources of anomalous diffusion on cell membranes: a Monte Carlo study. Biophys J 92:1975–1987.
113. Saxton, M. J. 1996. Anomalous diffusion due to binding: a Monte Carlo study. Biophys J 70:1250–1262.
114. Saxton, M. J. 2007. A biological interpretation of transient anomalous subdiffusion. II. Reaction kinetics. Biophys J 94:760–771.
115. Saxton, M. J. 2007. A biological interpretation of transient anomalous subdiffusion. I. Qualitative model. Biophys J 92:1178–1191.
116. Saxton, M. J. 1993. Lateral diffusion in an archipelago. Single-particle diffusion. Biophys J 64:1766–1780.

117. Martin, D. S., M. B. Forstner, and J. A. Kas. 2002. Apparent subdiffusion inherent to single particle tracking. Biophys J 83:2109–2117.
118. Sako, Y., and A. Kusumi. 1995. Barriers for lateral diffusion of transferrin receptor in the plasma membrane as characterized by receptor dragging by laser tweezers: fence versus tether. J Cell Biol 129: 1559–1574.
119. Daumas, F., N. Destainville, C. Millot, A. Lopez, D. Dean, and L. Salome. 2003. Confined diffusion without fences of a g-protein–coupled receptor as revealed by single particle tracking. Biophys J 84:356–366.
120. Lillemeier, B. F., J. R. Pfeiffer, Z. Surviladze, B. S. Wilson, and M. M. Davis. 2006. Plasma membrane-associated proteins are clustered into islands attached to the cytoskeleton. Proc Natl Acad Sci USA 103: 18992–18997.
121. King, M. R. 2004. Apparent 2-D diffusivity in a ruffled cell membrane. J Theor Biol 227:323–326.
122. Reister, E., and U. Seifert. 2005. Lateral diffusion of a protein on a fluctuating membrane. Europhys Lett 71:859–865.
123. Aizenbud, B. M., and N. D. Gershon. 1982. Diffusion of molecules on biological membranes of nonplanar form. A theoretical study. Biophys J 38:287–293.
124. Rustom, A., R. Saffrich, I. Markovic, P. Walther, and H. H. Gerdes. 2004. Nanotubular highways for intercellular organelle transport. Science 303:1007–1010.
125. Goulian, M., and S. M. Simon. 2000. Tracking single proteins within cells. Biophys J 79:2188–2198.
126. Destainville, N., and L. Salome. 2006. Quantification and correction of systematic errors due to detector time-averaging in single-molecule tracking experiments. Biophys J 90:L17–19.
127. Weiss, S. 1999. Fluorescence spectroscopy of single biomolecules. Science 283:1676–1683.
128. Baumgart, T., S. T. Hess, and W. W. Webb. 2003. Imaging coexisting fluid domains in biomembrane models coupling curvature and line tension. Nature 425:821–824.
129. Cognet, L., G. S. Harms, G. A. Blab, P. H. M. Lommerse, and T. Schmidt. 2000. Simultaneous dual-color and dual-polarization imaging of single molecules. Appl Phys Lett 77:4052–4054.
130. Jacobson, K., E. D. Sheets, and R. Simson. 1995. Revisiting the fluid mosaic model of membranes. Science 268:1441–1442.
131. Hac, A. E., H. M. Seeger, M. Fidorra, and T. Heimburg. 2005. Diffusion in two-component lipid membranes—a fluorescence correlation spectroscopy and Monte Carlo simulation study. Biophys J 88: 317–333.
132. Loose, M., E. Fischer-Friedrich, J. Ries, K. Kruse, and P. Schwille. 2008. Spatial regulators for bacterial cell division self-organize into surface waves *in vitro*. Science 320:789–792.
133. Benson, R. C., R. A. Meyer, M. E. Zaruba, and G. M. McKhann. 1979. Cellular autofluorescence—is it due to flavins? J Histochem Cytochem 27:44–48.
134. Konig, K., P. T. So, W. W. Mantulin, B. J. Tromberg, and E. Gratton. 1996. Two-photon excited lifetime imaging of autofluorescence in cells during UVA and NIR photostress. J Microsc 183:197–204.
135. Andersson, H., T. Baechi, M. Hoechl, and C. Richter. 1998. Autofluorescence of living cells. J Microsc 191(Pt 1):1–7.
136. Schnell, S. A., W. A. Staines, and M. W. Wessendorf. 1999. Reduction of lipofuscin-like autofluorescence in fluorescently labeled tissue. J Histochem Cytochem 47:719–730.
137. Moertelmaier, M. A., E. J. Kögler, J. Hesse, M. Sonnleitner, L. A. Huber, and G. J. Schütz. 2002. Single molecule microscopy in living cells: subtraction of autofluorescence based on two color recording. Single Mol. 3:225–231.
138. Seisenberger, G., M. U. Ried, T. Endress, H. Buning, M. Hallek, and C. Brauchle. 2001. Real-time single-molecule imaging of the infection pathway of an adeno-associated virus. Science 294:1929–1932.
139. van den Berg, C. W., T. Cinek, M. B. Hallett, V. Horejsi, and B. P. Morgan. 1995. Exogenous glycosyl phosphatidylinositol-anchored CD59 associates with kinases in membrane clusters on U937 cells and becomes Ca(2+)-signaling competent. J Cell Biol 131:669–677.
140. Shaner, N. C., P. A. Steinbach, and R. Y. Tsien. 2005. A guide to choosing fluorescent proteins. Nat Methods 2:905–909.
141. Gronemeyer, T., G. Godin, and K. Johnsson. 2005. Adding value to fusion proteins through covalent labelling. Curr Opin Biotechnol 16:453–458.
142. Freudenthaler, G., M. Axmann, H. Schindler, B. Pragl, H. G. Knaus, and G. J. Schütz. 2002. Ultrasensitive pharmacological characterisation of the voltage-gated potassium channel K(V)1.3 studied by single-molecule fluorescence microscopy. Histochem Cell Biol 117:197–202.
143. Nechyporuk-Zloy, V., P. Dieterich, H. Oberleithner, C. Stock, and A. Schwab. 2008. Dynamics of single potassium channel proteins in the plasma membrane of migrating cells. Am J Physiol Cell Physiol 294: C1096–1102.

144. Howarth, M., W. Liu, S. Puthenveetil, Y. Zheng, L. F. Marshall, M. M. Schmidt, K. D. Wittrup, M. G. Bawendi, and A. Y. Ting. 2008. Monovalent, reduced-size quantum dots for imaging receptors on living cells. Nat Methods 5:397–399.
145. Morrisett, J. D., H. J. Pownall, R. T. Plumlee, L. C. Smith, and Z. E. Zehner. 1975. Multiple thermotropic phase transitions in *Escherichia coli* membranes and membrane lipids. A comparison of results obtained by nitroxyl stearate paramagnetic resonance, pyrene excimer fluorescence, and enzyme activity measurements. J Biol Chem 250:6969–6976.
146. Brown, D. A., and J. K. Rose. 1992. Sorting of GPI-anchored proteins to glycolipid-enriched membrane subdomains during transport to the apical cell surface. Cell 68:533–544.
147. Melkonian, K. A., T. Chu, L. B. Tortorella, and D. A. Brown. 1995. Characterization of proteins in detergent-resistant membrane complexes from Madin-Darby canine kidney epithelial cells. Biochemistry 34: 16161–16170.
148. Lisanti, M. P., P. E. Scherer, J. Vidugiriene, Z. Tang, A. Hermanowski-Vosatka, Y. H. Tu, R. F. Cook, and M. Sargiacomo. 1994. Characterization of caveolin-rich membrane domains isolated from an endothelial-rich source: implications for human disease. J Cell Biol 126:111–126.
149. Horejsi, V., K. Drbal, M. Cebecauer, J. Cerny, T. Brdicka, P. Angelisova, and H. Stockinger. 1999. GPI-microdomains: a role in signalling via immunoreceptors. Immunol Today 20:356–361.
150. Brown, R. E. 1998. Sphingolipid organization in biomembranes: what physical studies of model membranes reveal. J Cell Sci 111(Pt 1):1–9.
151. Schroeder, R., E. London, and D. Brown. 1994. Interactions between saturated acyl chains confer detergent resistance on lipids and glycosylphosphatidylinositol (GPI)-anchored proteins: GPI-anchored proteins in liposomes and cells show similar behavior. Proc Natl Acad Sci USA 91:12130–12134.
152. Brown, D. A., and E. London. 1998. Structure and origin of ordered lipid domains in biological membranes. J Membr Biol 164:103–114.
153. Brown, D. A., and E. London. 1998. Functions of lipid rafts in biological membranes. Annu Rev Cell Dev Biol 14:111–136.
154. Resh, M. D. 1999. Fatty acylation of proteins: new insights into membrane targeting of myristoylated and palmitoylated proteins. Biochim Biophys Acta 1451:1–16.
155. Peirce, M., and H. Metzger. 2000. Detergent-resistant microdomains offer no refuge for proteins phosphorylated by the IgE receptor. J Biol Chem 275:34976–34982.
156. Kurzchalia, T. V., E. Hartmann, and P. Dupree. 1995. Guilt by insolubility—does a protein's detergent insolubility reflect a caveolar location? Trends Cell Biol 5:187–189.
157. Heerklotz, H. 2002. Triton promotes domain formation in lipid raft mixtures. Biophys J 83:2693–2701.
158. London, E., and D. A. Brown. 2000. Insolubility of lipids in triton X-100: physical origin and relationship to sphingolipid/cholesterol membrane domains (rafts). Biochim Biophys Acta 1508:182–195.
159. Li, X. M., J. M. Smaby, M. M. Momsen, H. L. Brockman, and R. E. Brown. 2000. Sphingomyelin interfacial behavior: the impact of changing acyl chain composition. Biophys J 78:1921–1931.
160. Edidin, M., S. C. Kuo, and M. P. Sheetz. 1991. Lateral movements of membrane glycoproteins restricted by dynamic cytoplasmic barriers. Science 254:1379–1382.
161. Lee, G. M., F. Zhang, A. Ishihara, C. L. McNeil, and K. A. Jacobson. 1993. Unconfined lateral diffusion and an estimate of pericellular matrix viscosity revealed by measuring the mobility of gold-tagged lipids. J Cell Biol 120:25–35.
162. Tomishige, M., Y. Sako, and A. Kusumi. 1998. Regulation mechanism of the lateral diffusion of band 3 in erythrocyte membranes by the membrane skeleton. J Cell Biol 142:989–1000.
163. Simson, R., B. Yang, S. E. Moore, P. Doherty, F. S. Walsh, and K. A. Jacobson. 1998. Structural mosaicism on the submicron scale in the plasma membrane. Biophys J 74:297–308.
164. Sako, Y., and A. Kusumi. 1994. Compartmentalized structure of the plasma membrane for receptor movements as revealed by a nanometer-level motion analysis. J Cell Biol 125:1251–1264.
165. Suzuki, K. G., T. K. Fujiwara, M. Edidin, and A. Kusumi. 2007. Dynamic recruitment of phospholipase C{gamma} at transiently immobilized GPI-anchored receptor clusters induces IP3-Ca2+ signaling: single-molecule tracking study 2. J Cell Biol 177:731–742.
166. Pike, L. J. 2006. Rafts defined. J Lipid Res 47:1597–1598.